sciendo

Civil and Environmental Engineering
Vol. 21, Issue 2, 1127-1138, DOI: 10.2478/cee-2025-0084

EXPERIMENTAL AND NUMERICAL INVESTIGATION ON THE FLEXURAL-COMPRESSION BEHAVIOR OF A NOVEL PREFABRICATED STEEL TUBE–CONCRETE COMPOSITE SHEAR WALL

Wenyan GENG [1,2], Dashuai WANG [1, 2, *]

[1] Zhengzhou Railway Vocational and Technical College, Zhengzhou 451460, China.
[2] Henan High-speed Railway Operation and Maintenance Engineering Research Centre, Zhengzhou 451460, China.
[*] corresponding author: ydmcsu@163.com

Abstract

This study proposes a novel prefabricated rectangular steel tube–concrete composite shear wall system, comprising square steel tube columns integrated with a concrete wall panel. Finite element simulations were performed to investigate the structural behaviour and assess the influence of key parameters, including steel tube strength, axial compression ratio, and shear-span ratio. The results demonstrate that the proposed shear wall exhibits a typical flexural–compression failure mode, characterized by yielding of the boundary steel tubes and localized buckling on the compression side. Parametric analyses reveal that increasing the steel tube strength significantly improves the load-bearing capacity, with both the characteristic load and corresponding displacement showing marked enhancement, thereby improving both strength and deformability. Higher axial compression ratios result in a steeper ascending branch in the load–displacement response, accompanied by reductions in yield and peak displacements. Moreover, while the ultimate load initially increases with axial compression ratio, it subsequently declines due to reduced confinement effectiveness and ductility. Conversely, an increased shear-span ratio leads to a decrease in peak load but enhances deformation capacity and overall ductility.

Keywords:

Composite shear wall;
Flexural-compression test;
Concrete-filled square steel tube column;
Flexural-compression behaviour.

1 Introduction

Shear wall structural systems have been extensively employed in high-rise buildings due to their superior lateral stiffness, high load-bearing capacity, and architectural versatility. However, traditional reinforced concrete shear walls exhibit several intrinsic drawbacks, including excessive self-weight, reduced construction efficiency, and unfavourable seismic failure modes, such as concrete crushing at corners and severe spalling. In recent years, the integration of novel materials into building structures has been increasingly explored to enhance mechanical performance [1,2], leading to greater diversity in shear wall configurations. To overcome the limitations of conventional designs and improve structural resilience, recent research has increasingly focused on steel–concrete composite shear wall systems. In particular, considerable efforts have been directed toward optimizing boundary element design through the incorporation of advanced components such as concrete-filled steel tube (CFST) columns, embedded steel tubular elements [3–5], and structural steel sections [6,7]. These modifications have demonstrated remarkable improvements in mechanical performance, as evidenced by numerous experimental and numerical investigations that have yielded substantial advancements in the field. Yüksel et al. [8] incorporated L-shaped steel sections as longitudinal reinforcement within the boundary elements of shear walls to address the insufficient lateral stiffness of conventional specimens. Pseudo-static tests revealed that the resulting hysteresis curves of the composite shear walls were significantly fuller, indicating enhanced energy dissipation capacity and ductility. Dan et al. [9] conducted seismic performance tests on five concrete shear wall specimens incorporating various types of embedded steel sections, along with one conventional reinforced concrete shear wall used as a reference. All specimens had a shear-span ratio of 2.6. The experimental results indicated that although all specimens exhibited similar flexural failure modes, the shear walls with embedded steel sections demonstrated superior load-bearing capacity and improved ductility compared to the conventional specimen. Ji et al. [10] conducted pseudo-static tests on two composite shear wall specimens incorporating embedded diagonal steel bracings. The wall panels featured flanged cross-sections to enhance flexural capacity while maintaining a shear-dominated failure mode. Test results revealed that concrete spalling around inclined shear cracks reduced the confinement of the embedded bracings, leading to local buckling. Although both types of bracings-steel plates and I-shaped steel-exhibited post-yield buckling and contributed comparably to the shear capacity of the walls, the study recommended steel plate bracings due to their simpler end connections, improved construction quality, and higher installation efficiency. Emami et al. [11] performed seismic tests on composite shear walls incorporating flat and corrugated steel plates arranged in both horizontal and vertical orientations. The results indicated that flat steel plate shear walls exhibited slightly higher load-bearing capacity. Nevertheless, both configurations effectively suppressed the pinching phenomenon in the hysteresis curves, resulting in fuller and more stable energy dissipation behaviour.

The aforementioned studies demonstrate that the integration of steel sections or steel plates into concrete shear walls can significantly improve their load-bearing capacity, ductility, and energy dissipation performance. However, several limitations remain. The bond between steel and concrete is relatively weak, and noticeable buckling of the steel plates often occurs in the later stages of loading. The inclusion of embedded steel components and reinforcement complicates the internal configuration of the shear wall, necessitating high construction precision. Moreover, once the concrete cracks and subsequently spalls, the exposed steel elements become more susceptible to corrosive environments, thereby increasing maintenance demands. These challenges, to some extent, hinder the further development and widespread implementation of such composite shear wall systems. Wu et al. [12] proposed a precast steel tube–concrete composite shear wall system in which steel tubes fully replaced conventional longitudinal reinforcement in the boundary elements. Experimental results demonstrated that this configuration exhibited excellent deformation capacity and shear resistance under applied loading, highlighting its potential for future structural applications. Zhou et al. [13] designed and conducted a series of seismic tests on high-strength CFST composite shear walls. The presence of steel tubes significantly enhanced the flexural stiffness of the specimens, leading to substantial improvements in the overall seismic performance. The vertical load-bearing capacity of the specimens remained stable, and even under high axial compression ratios, the specimens maintained favourable ductility and energy dissipation capacity. Based on these findings, the study recommended raising the axial compression ratio limit for high-strength CFST composite shear walls. You et al. [14] investigated an innovative composite structure consisting of steel fibre-reinforced concrete (SFRC) shear walls with CFST columns. Based on shear mechanism analysis, they proposed a softened strut-and-tie model (SSTM) to calculate the shear strength of these composite walls. The model incorporates diagonal, horizontal, and vertical mechanisms, accounting for contributions from concrete, reinforcement, and steel fibres in the SFRC web. Validation against 24 test specimens showed good agreement with experimental results. The study demonstrated that randomly distributed steel fibres could be effectively treated as equivalent reinforcement in shear strength analysis, confirming the SSTM as a reliable method for predicting shear capacity in SFRC-CFST composite walls. Cao et al. [15] conducted seismic tests on three types of shear wall specimens: a conventional reinforced concrete wall, a shear wall with steel tube–concrete columns, and a CFST composite wall incorporating steel plate bracing trusses. The results demonstrated that both the steel tube–concrete columns and the steel plate trusses significantly enhanced the structural performance. In particular, the inclusion of steel plate trusses effectively delayed stiffness degradation, restrained crack propagation, and promoted a more uniform crack distribution. Among the tested configurations, the composite wall with steel tube columns and steel plate trusses exhibited the most favorable seismic performance. Ren et al. [16] developed an innovative composite shear wall system by integrating FRP-confined concrete cores into the CFST boundary elements of multi-cavity steel tube walls (MCSTWs). Cyclic loading tests were performed on five specimens—including GFRP-enhanced CFSTs, conventional MCSTWs, and FRP-confined MCSTW variants. The results revealed that the proposed system exhibited markedly improved seismic performance, with a 30% increase in energy dissipation, more stable post-yield behavior, and a 25% enhancement in load-bearing capacity compared to traditional walls. These findings underscore the system's potential for application in seismic-resistant high-rise construction. Compared with conventional reinforced concrete shear walls, CFST shear walls effectively mitigate crack development while maintaining high load-bearing capacity, flexural stiffness, and deformation capacity. This enhanced performance is primarily attributed to the synergistic interaction between the steel tube and the concrete core, wherein the confining effect of the steel tube significantly improves the overall mechanical response of the system [17,18]. Under cyclic loading conditions, CFST shear walls are particularly effective in delaying crack propagation and suppressing local buckling, thereby exhibiting superior seismic energy dissipation capacity relative to conventional steel–concrete structural systems.

In summary, conventional shear wall structures are characterized by considerable self-weight and are prone to damage at the boundary regions. To address these limitations, researchers have proposed various forms of composite shear walls and conducted extensive studies, revealing that such systems exhibit significantly improved mechanical performance compared to traditional reinforced concrete shear walls. However, the high cost of steel, the substantial amount of structural steel required, and the associated construction complexity often led to increased overall construction costs and challenges in practical implementation. To overcome these limitations, this study proposes a simplified composite shear wall system composed of prefabricated square CFST columns connected to a reinforced concrete wall panel, as illustrated in Fig. 1. To reduce the overall dimensions and self-weight of the shear wall, square CFST components are employed on both sides of the wall to fully exploit the mechanical advantages of CFSTs, while the central portion of the wall adopts a conventional reinforced concrete configuration. The steel tubes on either side are connected via end plates at the top and bottom, and a row of shear studs is welded along the steel tubes to enhance the composite action between the concrete wall panel and the CFST columns. To investigate the structural behaviour of this novel system, the present study simulates realistic engineering conditions to analyse the failure modes and load-bearing performance of the proposed shear wall under combined axial and bending loading. Finite element parametric analyses are conducted to provide valuable insights and design recommendations for this composite shear wall configuration.

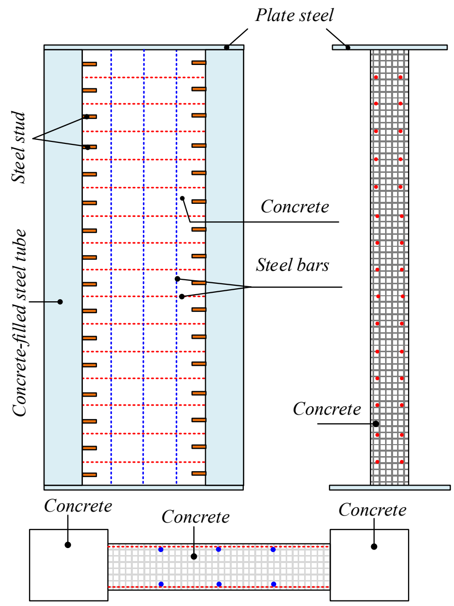

Fig. 1: Structural configuration of the CFST composite shear wall.

2 Experimental design and testing

2.1 Experimental model design

To investigate the mechanical behaviour of the shear wall illustrated in Fig. 1, a full-scale specimen was designed based on practical engineering applications. The detailed dimensions and reinforcement layout of the specimen are presented in Fig. 2. The shear wall has a total width of 1000 mm and a height of 3000 mm. Two square steel tubes, each with a side length of 200 mm and a wall thickness of 8 mm, were positioned at both edges of the wall. These steel tubes, fabricated from Q355B-grade steel, were filled with C30-grade concrete. The central portion of the shear wall comprises a reinforced concrete panel with a width of 600 mm and a thickness of 130 mm. The horizontal and vertical distributed reinforcements in this panel consisted of HRB400-grade steel bars with diameters of 10 mm and 12 mm, respectively, arranged in a two-way layout with 200 mm spacing. Material property tests were conducted in accordance with relevant standards. The tensile properties of the steel tubes and reinforcing bars are summarized in Table 1. To ensure proper construction sequencing, the concrete in the shear wall specimen was cast in two stages: first, the central reinforced concrete panel was cast using formwork, followed by concrete infill of the edge square steel tube columns seven days later.

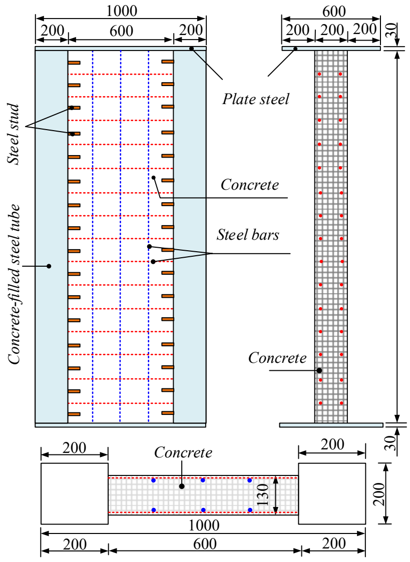

Fig. 2: Configuration and geometric dimensions of the test specimen.

Table 1: Properties of steel plates and reinforcement.

Materials	Yield strength of steel fy [Mpa]	Tensile strength fu [Mpa]	Elongation δ [%]
Steel tube	385.5	489.6	28.71%
C10 steel bar	442.1	547.6	17.81%
C12 steel bar	420.4	519.5	18.06%

2.2 Experimental setup and loading scheme

After 28 days of curing, the shear wall specimen was transported to the laboratory for testing. As illustrated in Fig. 3, horizontal loading was applied using a 1000 kN electro-hydraulic servo actuator, which was connected to the loading beam at the right end of the specimen via a swivel joint. Vertical loading was applied by an additional 1000 kN hydraulic servo actuator. Following preloading, a constant axial compressive load was applied and maintained throughout the test. Prior to yielding, the specimen was subjected to force-controlled loading. Yielding was defined as the point at which the strain gauges installed at the base of the square steel tube columns reached the yield strain, with each load step held for five minutes. After yielding, the loading protocol was switched to displacement-controlled mode, with increments of 5 mm per cycle. The test was terminated when any of the following conditions were met: visible specimen failure, load dropped below 85% of the peak value, or further loading became unfeasible.

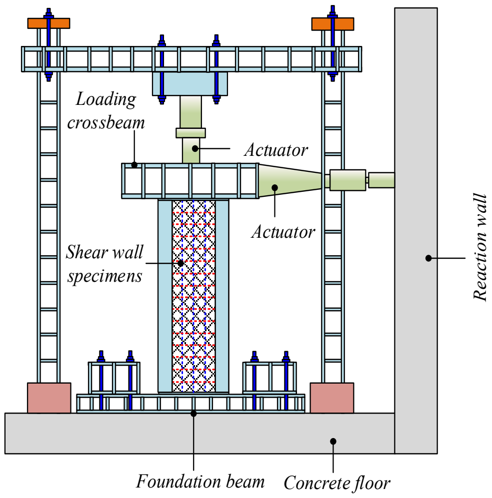

Fig. 3: Schematic diagram of the test loading setup.

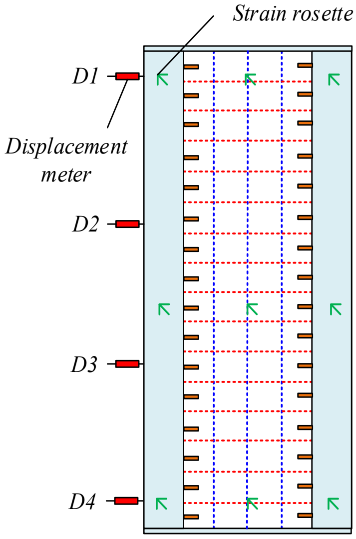

Fig. 4: Measurement point arrangement of the shear wall.

The experimental measurements included strain and displacement data at critical locations of the shear wall. The displacement monitoring primarily focused on recording lateral deformations, with the following sensor arrangement: Displacement measurement: Four linear variable displacement transducers (LVDTs), labelled D1 to D4, were vertically installed on the left CFST column at four different elevations to measure lateral displacements under various loading stages. Strain measurement: Three rows of strain rosettes were vertically arranged on both the steel tube columns and concrete wall surface to investigate the vertical strain distribution along the wall height. The detailed configuration of the LVDTs and strain rosettes is presented in Fig. 4.

3 FE simulations

To further elucidate the load-bearing mechanisms and failure modes of the shear wall specimens and to facilitate subsequent parametric analyses, numerical simulations were conducted using the ABAQUS finite element software. The simulation results were compared with corresponding experimental data to validate the model. As illustrated in Fig. 5, the finite element model adopted the following modeling strategies: the concrete was represented using three-dimensional eight-node reduced integration solid elements (C3D8R), while the steel tubes and the connecting steel plates at the top and bottom of the specimens were modeled using shell elements (S4R). Reinforcement bars were modeled with truss elements (T3D2) and embedded into the concrete solid elements in the mid-wall region. The welding connections between the steel tubes and steel plates were simulated using tie constraints, and the interaction between the concrete and steel components was modeled through appropriate contact definitions.

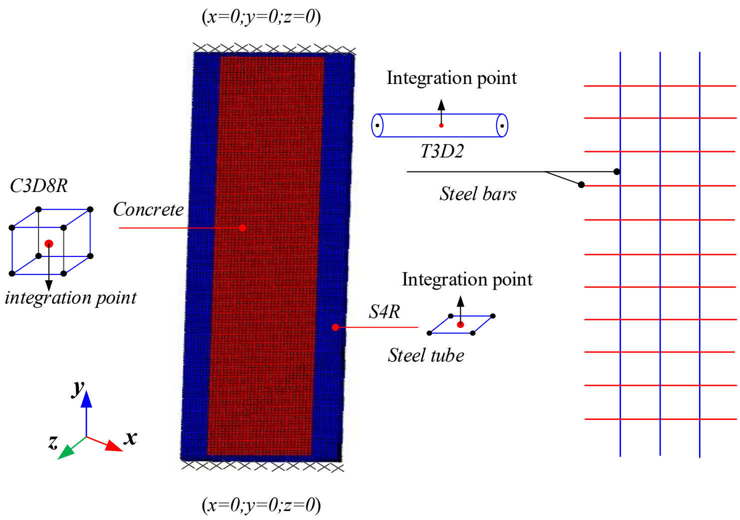

Fig. 5: FE model.

The concrete material behavior was captured using the Concrete Damage Plasticity (CDP) model. The evolution of the yield surface was governed by two primary hardening variables: equivalent tensile plastic strain and equivalent compressive plastic strain. The cracking and crushing behavior of the concrete was represented by progressively increasing tensile and compressive hardening parameters. The uniaxial tensile and compressive stress-strain relationships adopted for concrete are shown in Fig. 6, while the key parameters for the CDP failure criterion are summarized in Table 2.

Table 2: CDP model failure criterion parameters.

Dilation angle [°]	Eccentricity	Biaxial to uniaxial compressive strength ratio	Stress invariant ratio	Viscosity parameter
15	0.1	1.16	2/3	0.005

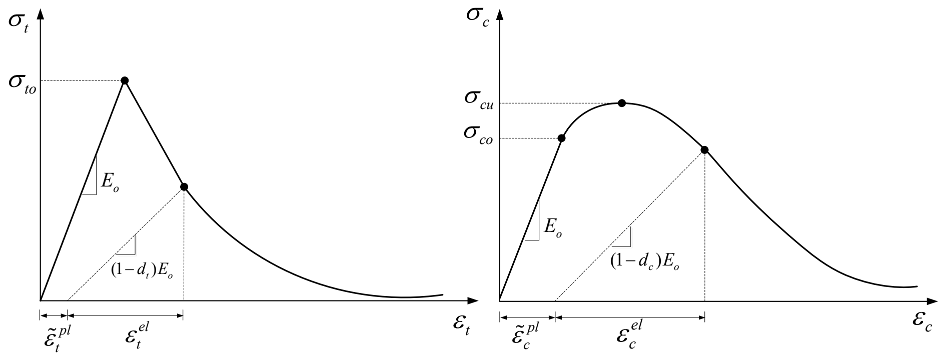

Fig. 6: Uniaxial tensile and compressive stress-strain relationships of concrete. (a) Tension; (b) Compression.

In the finite element model, both steel and reinforcement were modeled using an ideal elastic-perfectly plastic constitutive law. This model assumes that the material exhibits nearly linear elastic behavior before reaching the yield strength, where stress increases proportionally with strain. Once the yield strength is reached or exceeded, the material enters a plastic state, in which the stress remains constant despite continued strain development, thereby reflecting the characteristics of an ideal plastic material. The corresponding stress-strain relationship is illustrated in Fig. 7. In the model, the elastic modulus of steel was defined as 2.1×10^5 MPa, with a density of 7800 kg/m^3 and a Poisson's ratio of 0.3. Material strength parameters were based on experimentally measured values. Given that significant lateral displacement occurred during testing, the loading protocol in the finite element simulation was implemented by applying prescribed displacements. The bottom of the foundation beam was fully fixed, while the out-of-plane translational degree of freedom in the X direction and the rotational degrees of freedom about the Y and Z axes at the specimen top were constrained to replicate the boundary conditions observed during the physical experiment.

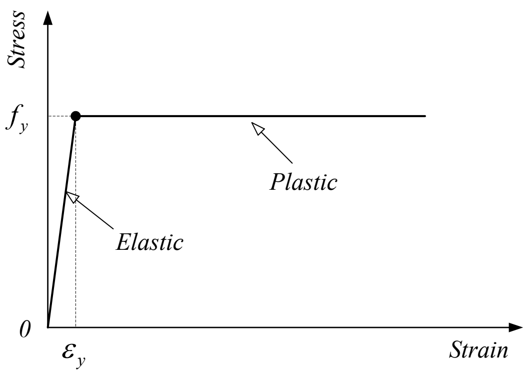

Fig. 7: Stress-strain model of steel.

4 Results and discussion

4.1 Experimental results and analysis

In the initial loading stage, the specimen remained in the elastic phase, exhibiting no significant visible changes. When the horizontal load reached 160 kN, an approximately horizontal crack appeared on the tension side of the shear wall, approximately 380 mm above the wall base, as shown in Fig. 8. As the load increased to 332 kN, local buckling was observed at the base of the compressed square steel tube column, indicating that the steel tube had yielded. At this point, the loading mode was switched from force control to displacement control. With further increases in the horizontal load, additional horizontal cracks formed in the concrete wall and began to propagate diagonally downward, eventually developing into flexure-shear inclined cracks. When the top displacement reached 48.3 mm, the square steel tube column on the tension side yielded, corresponding to a horizontal load of 366 kN. As the top displacement increased to 86.2 mm, the horizontal load peaked at 453 kN. Subsequently, the load entered a plateau phase.

At a top displacement of 116.3 mm, a loud sound was emitted from the specimen, accompanied by tearing of the outermost weld seam at the base of the tension-side square steel tube column, and pronounced buckling of the compression-side column. The entire wall structure exhibited noticeable tilting, marking the end of the test. The final failure mode is illustrated in Fig. 8. The composite shear wall specimen experienced a flexural-compression failure. Prior to failure, both square steel tube columns at the ends had reached their yield strain. The dominant failure characteristics included local buckling at the base of the compression-side column, with varying degrees of wave-like deformation. No significant spalling of concrete was observed, though the tension-side of the wall exhibited slight uplift, and the entire specimen showed visible lateral displacement.

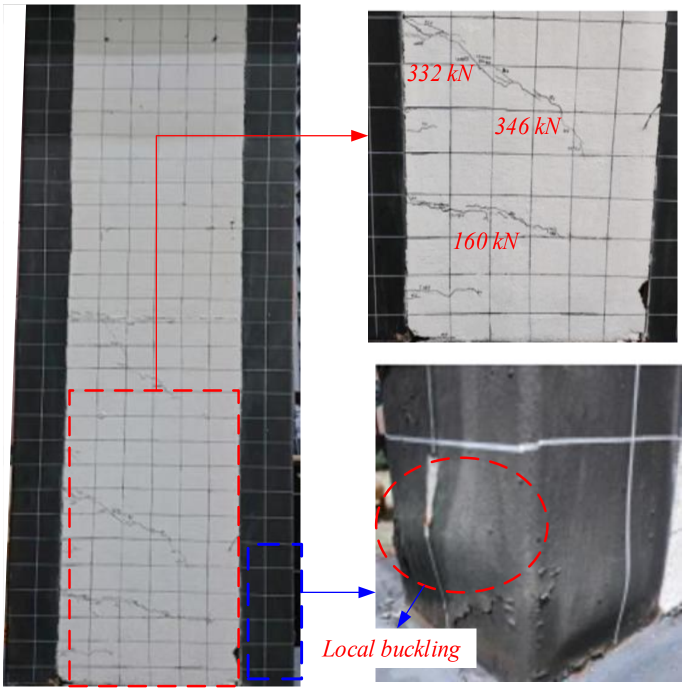

Fig. 8: Final failure mode and crack distribution of the specimen.

4.2 Comparison of experimental and numerical results

To further elucidate the failure mechanism of the shear wall proposed in this study, a comparative analysis was conducted between the horizontal load-displacement curves obtained from the experiments and those derived from FE simulations at each measurement point, as shown in Fig. 9. The results indicate a good agreement between the FE simulations and experimental data. Under constant axial compression and increasing lateral loads, the composite shear wall exhibited a typical flexural-dominant failure mode, and its failure process can be broadly divided into three stages: (1) Elastic stage: During this initial phase, no visible damage was observed on the specimen surface, and the load-displacement curve exhibited linear growth. (2) Elastic-plastic stage: As the lateral load increased, initial cracking occurred in the concrete wall, and the specimen entered the elastic-plastic phase. The load-displacement curve began to show nonlinear characteristics. With continued loading, local buckling occurred in the compressed square steel tube columns. (3) Failure stage: The cracks in the concrete wall propagated further, and the overall stiffness of the specimen gradually decreased. The load-displacement curve began to deviate from its original linear trend and sloped toward the displacement axis. After yielding of the square steel tubes, the load continued to increase and reached a peak. Despite the large lateral displacement at peak load, the post-peak strength degradation was relatively slow, indicating that the shear wall possessed excellent deformation capacity. Furthermore, Table 3 summarizes the shear capacities of the shear wall specimens obtained from both the experiments and FE simulations. The deviation between the simulated and experimental results was only 8.57%, further confirming the accuracy of the finite element modeling approach and its applicability for subsequent mechanical performance analysis of the proposed shear wall system.

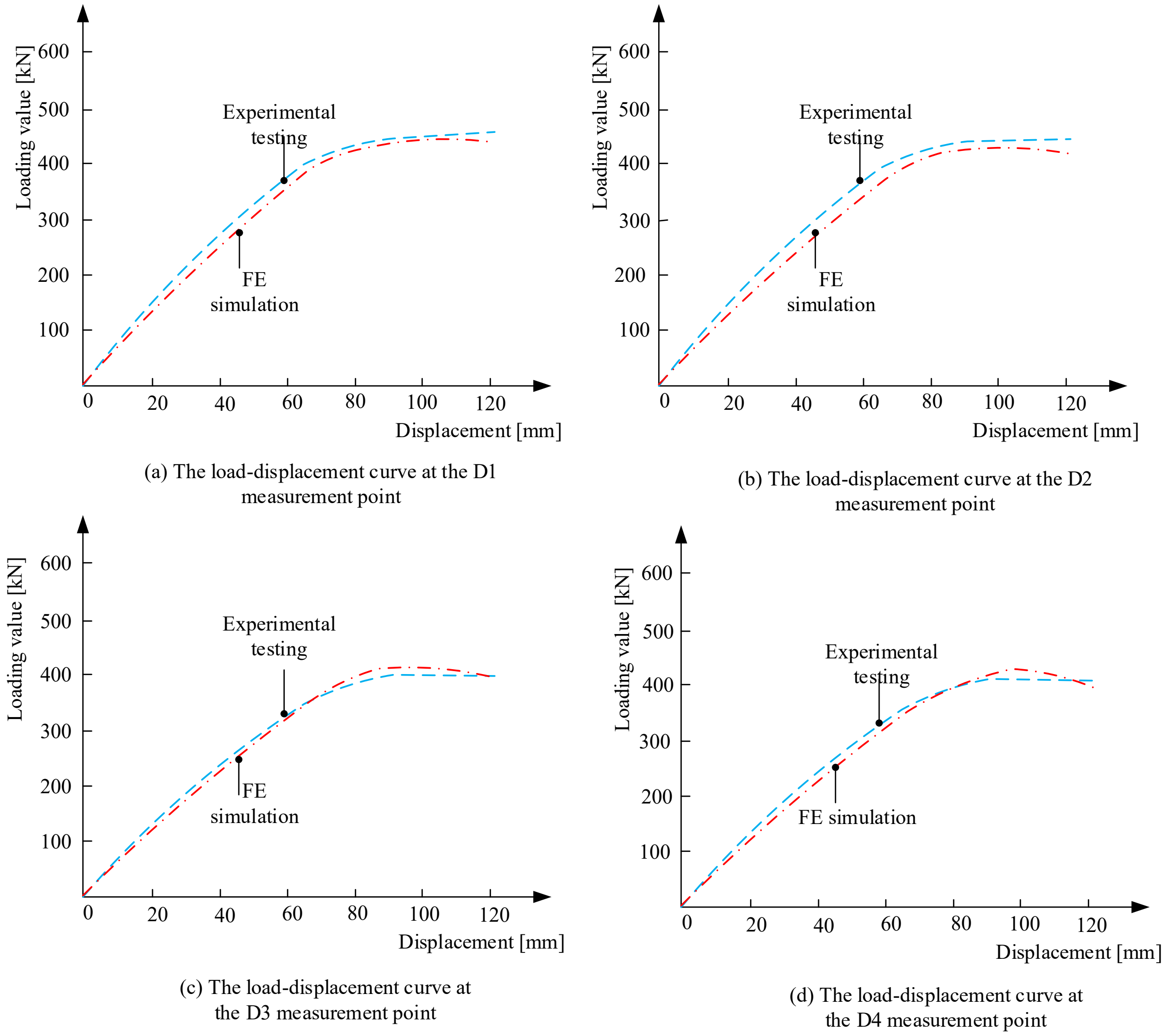

(a) The load-displacement curve at the D1 measurement point

(b) The load-displacement curve at the D2 measurement point

(c) The load-displacement curve at the D3 measurement point

(d) The load-displacement curve at the D4 measurement point

Fig. 9: Load-displacement curves of specimens obtained from finite element analysis and experimental measurements at measurement points. (a) The load-displacement curve at the D1 measurement point; (b) The load-displacement curve at the D2 measurement point; (c) The load-displacement curve at the D3 measurement point; (d) The load-displacement curve at the D4 measurement point.

Table 3: Comparison of bearing capacity between FE analysis and experiment.

Bearing capacity	FE value [kN]	Experimental value [kN]	Error [%]
	449	487.5	8.57%

5 Parametric analyses

Based on the aforementioned experimental and finite element simulation results, it is evident that under combined axial and lateral loading, the composite shear wall specimen primarily exhibited a flexural-compression failure mode. Before failure, both square steel tube columns at the wall ends had reached their yield strain. The dominant failure characteristics included local buckling at the base of the compression-side column, characterized by varying degrees of wave-like deformation. This indicates that the strength of the steel tube is a critical factor influencing the shear wall's load-bearing capacity.

Moreover, to ensure adequate ductility and collapse resistance, limitations are typically imposed on the axial compression ratio in high-rise shear wall structures. Additionally, the shear-span ratio plays a critical role in influencing the mechanical behavior of shear walls, particularly in governing the transition between shear-dominated and flexure-dominated failure modes. By varying the shear span-to-depth ratio, it becomes possible to systematically evaluate its effects on load-bearing capacity, deformation characteristics, and failure mechanisms. Therefore, in this chapter, a parametric analysis is conducted based on finite element simulations to investigate the influence of three key parameters-steel tube strength, axial compression ratio, and shear-span ratio on the mechanical performance of the composite shear wall.

5.1. Steel tube strength

As indicated by the experimental results, the square steel tube columns at the base of both sides of the shear wall specimen yielded prior to reaching the ultimate load state. This highlights that the strength grade of the steel used in the tubes is a critical factor influencing the flexural-compression behavior of the composite shear wall. To investigate the influence of steel tube strength on the structural performance of the shear wall, finite element models were developed based on the experimental specimen dimensions. The steel strength grades were varied among Q235, Q355 (baseline), and Q460, while keeping all other parameters constant. The axial compression ratio was set at 0.12. Load-displacement curves were obtained through numerical simulation, as shown in Fig. 10. The results indicate that replacing Q355 with Q235 steel reduced the yield load by 13.7% and the peak load by 9.16%. Conversely, using Q460 steel increased the yield load by 18.42% and the peak load by 11.69%. Furthermore, Fig. 10 shows that the initial elastic stiffness of the shear walls did not vary significantly with different steel strength grades. However, as displacement increased, both the characteristic loads and the corresponding characteristic displacements increased with steel strength, suggesting that higher-strength steel can significantly enhance both the load-bearing and deformation capacity of the shear wall. In addition, the post-peak softening behavior became more gradual with increasing steel strength, indicating an improvement in the ductility and energy dissipation capacity of the structure.

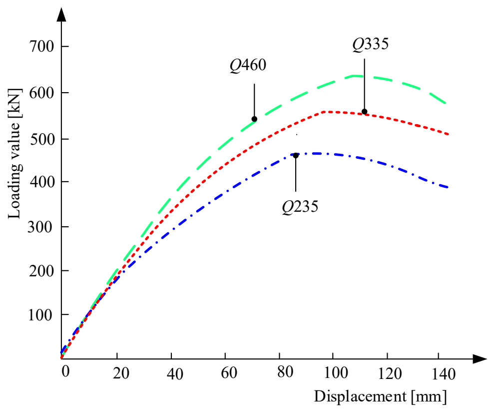

Fig. 10: Load－displacement curves of shear walls with different steel strength grades.

5.2 Axial compression ratio

To ensure sufficient ductility and collapse resistance, the axial compression ratio of shear walls in high-rise buildings is typically limited. Based on the FE model of the specimen, this study investigates the effect of different axial compression ratios while keeping all other parameters constant. The axial compression ratio was varied as 0.24, 0.36, 0.48, and 0.60. The yield points of each shear wall model were determined using the general yield moment method. The corresponding yield and peak loads for each case are summarized in Table 4.

Table 4: Characteristic load values of shear wall under different axial compression ratios.

Axial Compression Ratio	Yield Load [kN]	Peak Load [kN]
0.12	329.12	538.21
0.24	356.31	564.12
0.36	367.38	606.27
0.48	392.13	622.19

From Table 4, it can be observed that increasing the axial compression ratio from 0.12 to 0.36 significantly enhances both the yield and peak loads of the composite shear wall. Specifically, when the ratio increased from 0.12 to 0.24, the yield and peak loads increased by 7.4% and 5.4%, respectively. Further increasing the ratio from 0.24 to 0.36 resulted in additional increases of 3.4% and 8.1%, respectively. As the axial compression ratio rose from 0.36 to 0.48, the yield and peak loads increased by 6.3% and 2.7%. These results indicate that, within a certain range, increasing the axial compression ratio enhances the load-bearing capacity of the shear wall; however, the rate of improvement progressively decreases. Notably, when the axial compression ratio increased from 0.48 to 0.60, the yield load still exhibited a slight increase of approximately 3.9%, but the peak load began to decline.

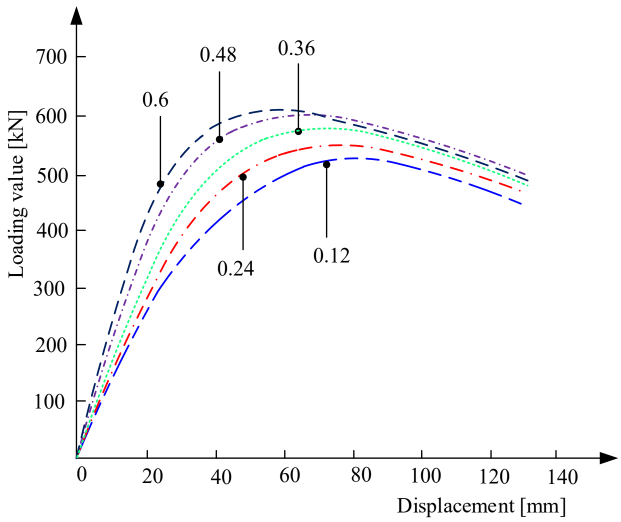

Fig. 11: Load – displacement curves of shear walls under different axial compression ratios.

Fig. 11 presents the load-displacement curves of the specimens under varying axial compression ratios. As shown, increasing the axial compression ratio significantly steepens the slope of the elastic-plastic ascending branch, and both the yield and peak displacements decrease accordingly. Moreover, in the post-peak stage, the descending branch becomes increasingly steep as the axial compression ratio increases, indicating a reduction in ductility. The ultimate load initially increases with the axial compression ratio, but then declines beyond a certain threshold. This trend is primarily attributed to the increased vertical load associated with higher axial compression ratios, which accelerates failure in the shear wall specimen. Under excessive axial loads, the confinement effect of the square steel tubes on the core concrete diminishes, thereby reducing the ductility and deformation capacity of the shear wall.

5.3. Shear-span ratio

To investigate the influence of the shear-span ratio on the mechanical behavior of the composite shear wall, a series of finite element simulations were conducted based on the geometric dimensions of the tested model. The axial compression ratio was fixed at 0.12, while the shear-span ratios were varied as 1.76, 2.01, 2.35, and 2.82. The corresponding load-displacement curves obtained from the simulations are presented in Fig. 12. As illustrated in Fig. 12, an increase in the shear-span ratio results in a noticeable decrease in the peak load of the shear wall. However, the characteristic displacement associated with both the yield and peak points is delayed with increasing shear-span ratio. This indicates that the shear-span ratio plays a critical role not only in the load-bearing capacity but also in the deformation capacity of shear walls. Moreover, the post-peak descending branch of the load-displacement curve becomes progressively less steep as the shear-span ratio increases, indicating a significant improvement in ductility. These findings suggest that shear-span ratio has a dual influence: while higher ratios may reduce peak strength, they can simultaneously enhance the overall deformation capacity and energy dissipation capability of the system.

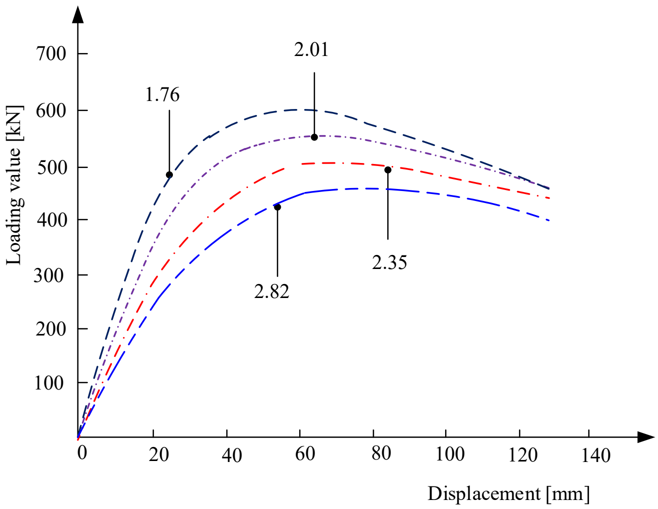

Fig. 12: Load-displacement curves of shear walls with varying shear-span ratios.

6 Conclusion

In this study, a novel rectangular steel tube–concrete composite shear wall was proposed. Its mechanical performance and failure characteristics under horizontal and axial loading were investigated through experimental tests and finite element simulations. Furthermore, a parametric study was conducted to examine the influence of steel strength, axial compression ratio, and shear-span ratio on the structural behaviour. The main conclusions are summarized as follows:

1) The proposed rectangular steel tube-concrete composite shear wall exhibited flexural-compression failure under combined horizontal and axial loading. Prior to failure, both end square steel tube columns reached their yield strain. The dominant failure mode was characterized by local buckling at the base of the compression-side column, manifesting as wave-like deformations.

2) The parametric analysis showed that increasing the strength of the square steel tube significantly enhances the load-bearing capacity of the specimen. In the initial elastic stage, the difference in stiffness between walls constructed with different steel grades was negligible. However, as displacement increased, both the characteristic load and the corresponding displacement increased with higher steel strength, indicating that steel grade plays a critical role in enhancing both the strength and deformation capacity of the shear wall. Moreover, the post-peak descending branch of the load–displacement curve became less steep as steel strength increased, demonstrating improved ductility.

3) With increasing axial compression ratio, the slope of the elastic–plastic ascending branch of the load–displacement curve increased markedly, while the displacements corresponding to the yield and peak points decreased. Additionally, at higher axial compression ratios, the post-peak descending segment of the curve became steeper, and the ultimate load followed a trend of initially increasing and then decreasing. This behaviour is attributed to excessive axial loads that diminish the confining effect of the steel tube on the inner concrete, leading to reduced ductility and deformation capacity. Therefore, a reasonable axial compression ratio is recommended in design to balance strength and ductility.

4) The parametric results revealed that as the shear-span ratio increased, the peak load of the shear wall decreased significantly. However, the characteristic displacements at the yield and peak points were delayed, suggesting that shear-span ratio is also a key factor in improving deformation capacity. Additionally, the post-peak descending branch became less steep with increasing shear-span ratio, indicating notable improvement in ductility as shear-span ratio increases.

Acknowledgement

No additional acknowledgments are required for this work.

References

[1] Al-BAGHDADI, H.M., & KADHUM, M.M. (2025). Performance and Mechanical Properties of Environmentally Engineered Cementitious Composites Produced from Local Waste. Civil and Environmental Engineering, 0(0), 2025. https://doi.org/10.2478/cee-2025-0029.

[2] ATIEA, H.M.., ALBAHRANI, H.S., ALLABAN, M.F., ALHADITHI, A.I. & JABAL, Q.A. (2025). Ceramic Waste as Fine and Coarse Aggregates for Sustainable Environment and Fire-Resistant Buildings. Civil and Environmental Engineering, 0(0), 2025. https://doi.org/10.2478/cee-2025-0040.
[3] ZHANG, H. X., PENG, Q., & ZHAO, L. X. (2015). The statement of research progress in embedded steel plate shear wall. Applied Mechanics and Materials. 638-640, 287-291.
[4] BAI, L., ZHANG, C., & XIONG, E. (2019). Investigations on the shear mechanism of steel-tube-reinforced concrete shear walls with a low shear-span ratio. KSCE Journal of Civil Engineering, 23(7), 2983-2996.
[5] ZHOU, J., FANG, X., & YAO, Z. (2018). Mechanical behavior of a steel tube-confined high-strength concrete shear wall under combined tensile and shear loading. Engineering Structures, 171(SEP.15), 673-685.
[6] SHAFAEI, S., FARAHBOD, F., & AYAZI, A. (2018). The wall–frame and the steel–concrete interactions in composite shear walls. The Structural Design of Tall and Special Buildings, 27(11).
[7] HANG, W., MAHDAVIAN, M., LAN, X., & YU, C. (2021). Cold-formed steel framed shear walls with in-frame corrugated steel sheathing. Journal of Structural Engineering.
[8] YÜKSEL, S.B, & ÜNAL, A. (2015). Experimental behavior of composite shear walls having L shape steel sections in boundary regions. *International Journal of Civil and Environmental Engineering.* 9, 747-752.
[9] DAN, D., FABIAN, A., & STOIAN, V. (2011). Theoretical and experimental study on composite steel–concrete shear walls with vertical steel encased profiles. Journal of Constructional Steel Research, 67(5), 800-813.
[10] JI, X., LEONG, T., QIAN, J., QI, W., & YANG, W. (2016). Cyclic shear behavior of composite walls with encased steel braces. Engineering Structures, 127(15), 117-128.
[11] EMAMI, F., MOFID, M., & VAFAI, A. (2013). Experimental study on cyclic behavior of trapezoidally corrugated steel shear walls. Engineering Structures, 48(48), 750-762.
[12] LI W., TIAN, Y., SU, Y.P., & CHEN, H.B. (2018). Seismic performance of precast composite shear walls reinforced by concrete-filled steel tubes. *Engineering Structures.* 162, 72-83.
[13] ZHOU, J., FANG, X., & JIANG, Y. Cyclic behavior of concrete-encased high-strength concrete-filled steel tube composite walls: An experiment. *Structural Concrete*. 2021, 22, 691-708.
[14] YOU, P., SONG, S., ZHANG, H., ZHANG, L., & WANG, Y. (2020). Shear strength prediction for SFRC shear wall with CFST columns by softened strut and tie model. Advances in Civil Engineering, 2020(4), 1-16.
[15] CAO, W., ZHANG, J., DONG, H., & WANG, M. (2011). Research on seismic performance of shear walls with concrete filled steel tube columns and concealed steel trusses. *Earthquake Engineering and Engineering Vibration*. 2011(10), 535-546.
[16] REN, F. M., LAI, C. L., GUO, J. Y., CHEN, G. M., TAO, Y., & XIE, P. (2022). Concrete-filled multicellular steel-tube shear walls with FRP tubes embedded in CFST: concept and seismic performance. Journal of Composites for Construction., 26(6), 23.
[17] HAN, L.H. Tests on stub columns of concrete-filled RHS sections. (2002). *Journal of constructional steel research.* 2002(58),353-372.
[18] INAI, E., MUKAI, A., KAI, M., TOKINOYA, H., FUKUMOTO, T., & MORI, K. (2004). Behavior of concrete-filled steel tube beam columns. Journal of Structural Engineering, 130(2), 189-202.